Electronic Structures of Nitridometalates: Molecular and Extended-Chain Ions

Michael T. Green and Timothy Hughbanks*

Department of Chemistry, Texas A&M University, College Station, Texas 77843-3255

Received June 11, 1993®

The unique structures of newly synthesized transition metal nitrides call for a description of their electronic structures that enables us to understand these compounds' bonding and properties. The compounds BaNiN, $M_2Li[Fe_2N_3]$ (M = Sr, Ba), and $M_2[FeN_2]$ (M = Ca, Sr) are examined through a local analysis of their band structure. The role of kinks in BaNiN is also studied as is the construction of $^1_\infty[(FeN_{3/2})_2^{5-}]$ chains through the condensation of $[Fe_2N_4]^{8-}$ dimers. The local description aids in understanding the role of metal–metal interactions in these systems. Using the results of this analysis, spin states and conductive properties of these novel compounds are discussed.

Introduction

Recent years have seen the synthesis of many structurally unusual transition metal nitrides. Ca_3MN_3 (M = V, Cr),[1-3] Ba_3FeN_3,[4] and $(Ca_3N)_2\{FeN_3\}$[5] all contain trigonal planar MN_3^{6-} ions. $Li_4[FeN_2]$ and $Sr_2[FeN_2]$ contain linear $[FeN_2]^{4-}$ ions, while $[Fe_2N_4]^{8-}$ ions are also found in the latter of these compounds as well as in $Ca_2[FeN_2]$.[6,7] Nonintersecting linear $^1_\infty[NiN^{2-}]$ chains criss-cross the structure of CaNiN,[8] while chains of the same connectivity are bent at every third nitrogen in BaNiN[9] (see Figures 1 and 2). More complex $^1_\infty[(FeN_{3/2})_2^{5-}]$ chains inhabit the structures of the compounds $M^{II}_2Li[Fe_2N_3]$ (M^{II} = Sr, Ba).[10] Each of these materials is interesting in that they show structural chemistry not commonly seen in transition metal complexes. The low coordination number of the metals, which allows for apparent multiple M–N bonding, is one of the most striking features of these compounds. The three-coordinate MN_3^{6-} ions were the subject of an earlier semiempirical and *ab initio* theoretical study from our laboratory and have few precedents in molecular chemistry.[11] The closest structural and electronic analogue to these ions in molecular chemistry is the osmium triimido complex $Os(N\text{-}2,6\text{-}C_6H_3\text{-}i\text{-}Pr_2)_3$,[12] in which the metal center is isoelectronic with vanadium in VN_3^{6-}.[12] Low coordination numbers for the transition metals are dictated by the relatively metal-rich compositions that these compounds adopt (e.g., if nitrogens in CaNiN are six-coordinate with respect to metals, the average coordination number of the metals by nitrogen can only be 3—the Ca centers have four nitrogen neighbors, and the Ni ions are two-coordinate). Coordination numbers 2 and 3 are exhibited by metals in oxoferrates and oxocobaltes that are rich in cations, e.g., $Na_4[MO_3]$ (M = Fe, Co), $Na_{10}[Co_4O_9]$, $K_2[NiO_2]$, and $RbNa_7[CoO_3]_2$.[13-18] While such low coordination numbers are a constraint imposed by the compounds' composition, the fact that compounds with these compositions exist at all argues for some special stabilization of low-coordinate transition metals by strong π-donors.

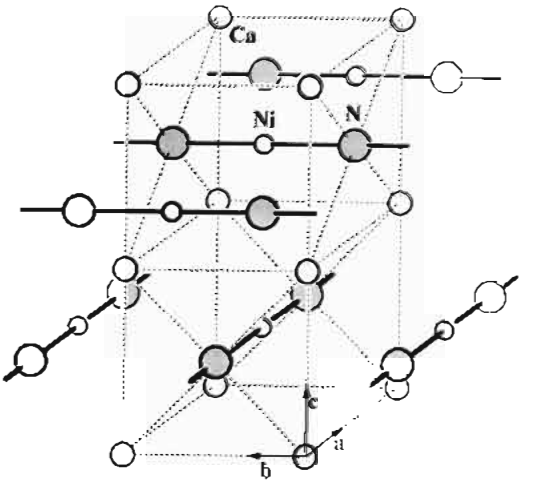

Figure 1. Crystal structure of CaNiN.

We are interested in bonding and structure–property relationships in these novel compounds. Unusual coordination environments require some new bonding prototypes and a need to develop useful working bonding models. These new structures also leave us with uncertain expectations for electronic and magnetic properties. In the present paper, we explore the links between the $[Fe_2N_4]^{8-}$ molecular ions and the $^1_\infty[(FeN_{3/2})_2^{5-}]$ extended-chain compounds. We also examine the role of kinks in the one-dimensional chains of BaNiN and compare this system with the linear-chain compound CaNiN.

Linear and Bent $^1_\infty[NiN^{2-}]$ Chains

Both BaNiN and CaNiN contain $^1_\infty[NiN^{2-}]$ chains (Figures 1 and 2); they are bent in the former and linear in the latter. The Ni–N distances in these compounds are very similar, 1.79 Å in CaNiN and an average of 1.80 Å in BaNiN. At the bend in BaNiN, the Ni–N–Ni angle is 83.9° and the Ni–Ni distance is 2.42 Å. An additional compound, $Ba_8Ni_6N_7$ $[=(Ba^{2+})_8(N^{3-})\text{-}^1_\infty(Ni_6N_6^{13-})]$, also contains chains which have bends at one-third of the nitrogens and which have helical coils—we will not treat this system in the present paper.[19]

* To whom correspondence should be addressed.
® Abstract published in *Advance ACS Abstracts,* November 1, 1993.

(1) Vennos, D. A.; Badding, M. E.; DiSalvo, F. J. *Inorg. Chem.* **1990**, *29*, 4059.
(2) Vennos, D. A.; DiSalvo, F. J. *J. Solid State Chem.* **1992**, *98*, 318, 322.
(3) Vennos, D. A.; DiSalvo, F. J. *J. Solid State Chem.* **1992**, *100*, 401.
(4) Höhn, P.; Kniep, R.; Rabenau, A. *Z. Kristallogr.* **1991**, *196*, 153.
(5) Cordier, G.; Höhn, P.; Kniep, R.; Rabenau, A. *Z. Anorg. Allg. Chem.* **1990**, *591*, 58.
(6) Gudat, A.; Kniep, R.; Rabenau, A. *Angew. Chem., Int. Ed. Engl.* **1991**, *30*, 199.
(7) Höhn, P.; Kniep, R. *Z Naturforsch., B* **1992**, *47*, 477.
(8) Chern, M. Y.; DiSalvo, F. J. *J. Solid State Chem.* **1990**, *88*, 459.
(9) Gudat, A.; Haag, S.; Kniep, R.; Rabenau, A. *J. Less-Common Met.* **1990**, *159*, L29.
(10) Höhn, P.; Haag, S.; Milius, W.; Kniep, R. *Angew. Chem., Int. Ed. Engl.* **1991**, *30*, 831.
(11) Yee, K. A.; Hughbanks, T. *Inorg. Chem.* **1992**, *31*, 1921.
(12) Anhaus, J. T.; Kee, T. P.; Schofield, M. H.; Schrock, R. R. *J. Am. Chem. Soc.* **1990**, *112*, 1642.
(13) Rieck, H.; Hoppe, R. *Z. Anorg. Allg. Chem.* **1977**, *437*, 95.
(14) Hoppe, V. R.; Rieck, H. *Z. Anorg. Allg. Chem.* **1977**, *437*, 95.
(15) Burow, W.; Hoppe, R. *Angew. Chem., Int. Ed. Engl.* **1979**, *18*, 542.
(16) Burow, W.; Hoppe, R. *Angew. Chem., Int. Ed. Engl.* **1979**, *18*, 61.
(17) Rieck, H.; Hoppe, R. *Z. Anorg. Allg. Chem.* **1973**, *400*, 311.
(18) Birx, J.; Hoppe, R. *Z. Anorg. Allg. Chem.* **1990**, *588*, 7.

0020-1669/93/1332-5611$04.00/0

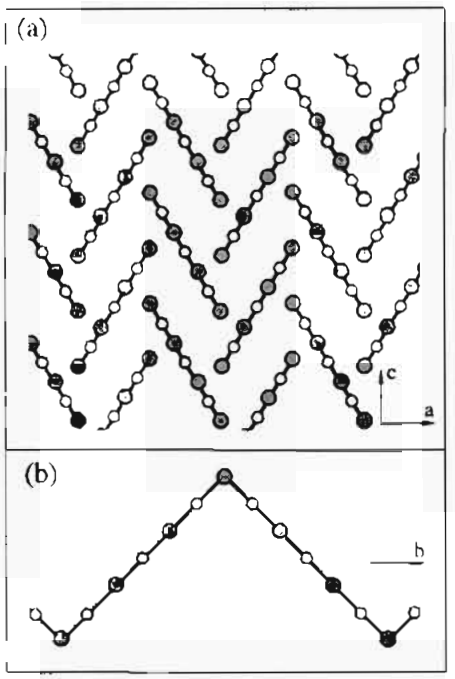

Figure 2. Structure and packing of the chains in BaNiN: (a) herringbone pattern of Ni–N chains as viewed down the *b* axis; (b) each Ni–N chain propagated along the *b* axis, planes in which the chains lie being inclined at angles of ±59° with respect to the *a* axis.

In analyzing the $M^{II}NiN$ compounds, it is first useful to reexamine the 1-D band structure of CaNiN. This compound is isotypic with SrLiN and YCoC,[20] the latter of which was shown by Hoffmann and co-workers to be a candidate for a Peierls distortion.[21] Subsequent investigations by Pickett and co-workers indicated that there is some weak through-space coupling of the $^1_\infty[NiN^{2-}]$ chains in CaNiN which stabilizes the undistorted chains in the CaNiN structure.[22] However, while these 3-D interactions serve to stabilize an undistorted structure, the underlying 1-D band structure persists and is easily recognizable. It is therefore useful for us to start with the 1-D band structure of CaNiN in our attempt to understand the role of kinks in BaNiN.

Figure 3 shows the energy bands for a $^1_\infty[NiN^{2-}]$ chain, calculated using the extended Hückel method. Details and parameters used in the calculations are described in the Appendix. In Figure 3, one can see the band structure of a linear M–N chain in the metal d region. The M *xy* and $x^2 - y^2$ orbitals are of δ symmetry, and as a result, no interaction with N p is possible. This results in the two degenerate nonbonding bands located at −13 eV. The M *xz* and *yz* orbitals, although of π symmetry, do not have the correct translational symmetry to interact with the N p at $k = 0$. However, as k increases, so does the M–N π interaction. The z^2 band is less disperse than the π band, which is initially surprising. This band is most easily understood as a nearly nonbonding z^2–s hybrid band. The z^2–s hybridization reduces the M–N interaction, thereby yielding a lower-lying and less disperse band. For a more detailed account, see the discussion by Hoffmann, Li, and Wheeler.[21]

We now derive the electronic structure of the zigzag $^1_\infty[NiN^{2-}]$ chains in BaNiN by distorting the linear-chain structure. This distortion gives a unit cell that is 6 times larger than that for the linear chain. We begin by introducing infinitesimal kinks at every third nitrogen. This yields a band structure which is just simply that for the linear cell—folded so that each band now has six branches. To help clarify this folding

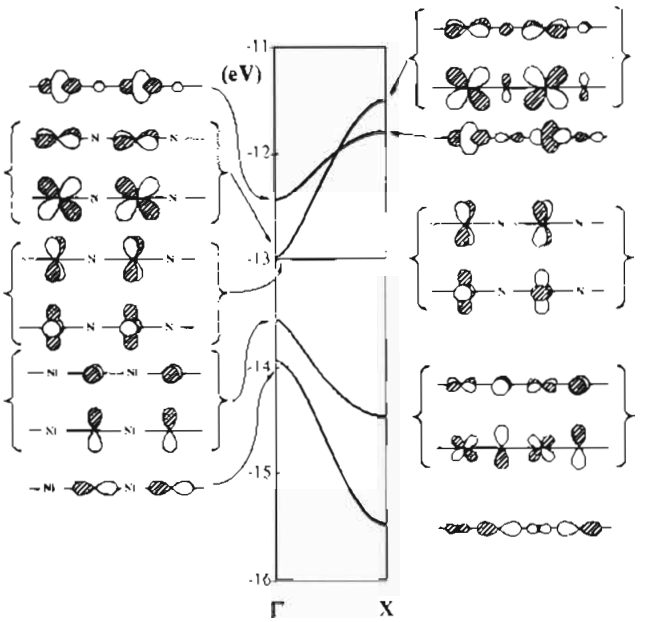

Figure 3. One-dimensional band structure of CaNiN. The orbitals are shown for each band at Γ ($k = 0$) and X ($k = \pi/a$).

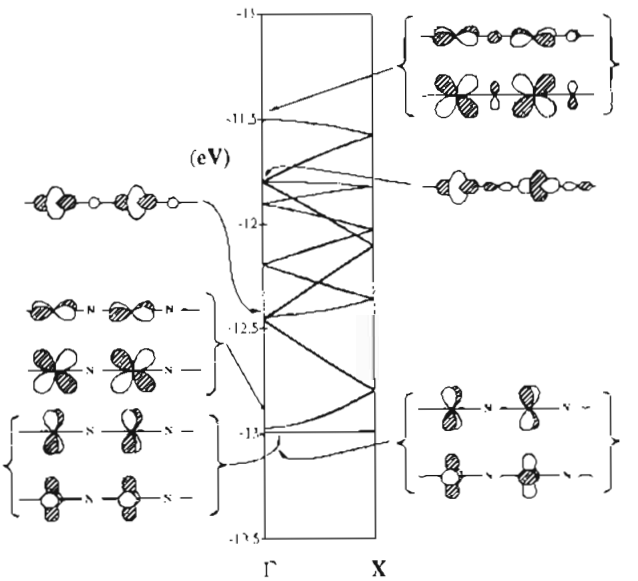

Figure 4. Band structure of the Ni–N chain bent so that infinitesimal kinks occur at every third nitrogen atom. The orbitals shown are the same as those in Figure 3.

process, we have marked the same wavefunctions in Figures 3 and 4. We now see what happens to some of these wavefunctions as the Ni–N–Ni angle is decreased.

First, we examine the set of degenerate δ bands. As the Ni–N–Ni angle decreases, the nickel atom on either side of the nitrogen at which the bend occurs are brought closer together, allowing for Ni–Ni σ and π type interactions (Figure 5). We therefore expect to see two sets of bonding bands pushed down as the Ni–N–Ni angle decreases, and a look at the band structure of BaNiN (left, Figure 6) reveals that this is what happens. Some of the bands which are pushed down (up) by Ni–Ni bonding (antibonding) interactions can be fruitfully interrogated by constructing local orbitals (Wannier functions) which reveal their Ni–Ni bonding character. Some details of local-orbital construction are given in the Appendix. Shown in Figure 6 are two local orbitals derived from bands descended from the linear-chain δ bands.

Both the Wannier orbitals constructed have Ni–Ni bonding character. The Wannier orbital with Ni–Ni π character (Figure

(19) Gudat, A.; Milius, W.; Haag, S.; Kniep, R.; Rabenau, A. *J. Less-Common Met.* **1991**, *168*, 305.
(20) Gerss, M. H.; Jeitschko, W. *Z. Naturforsch., B.* **1986**, *41*, 946.
(21) Hoffmann, R.; Li, J.; Wheeler, R. *J. Am. Chem. Soc.* **1987**, *109*, 6600.
(22) Massida, S.; Pickett, W. E.; Posternak, M. *Phys. Rev. B* **1991**, *44*, 1258.

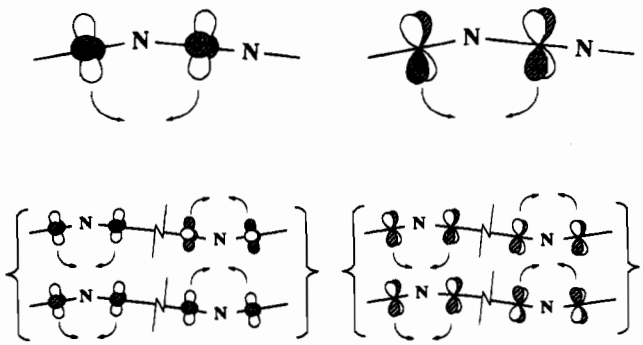

Figure 5. Illustration of the Ni–Ni interactions that are introduced as the Ni–N chain is bent.

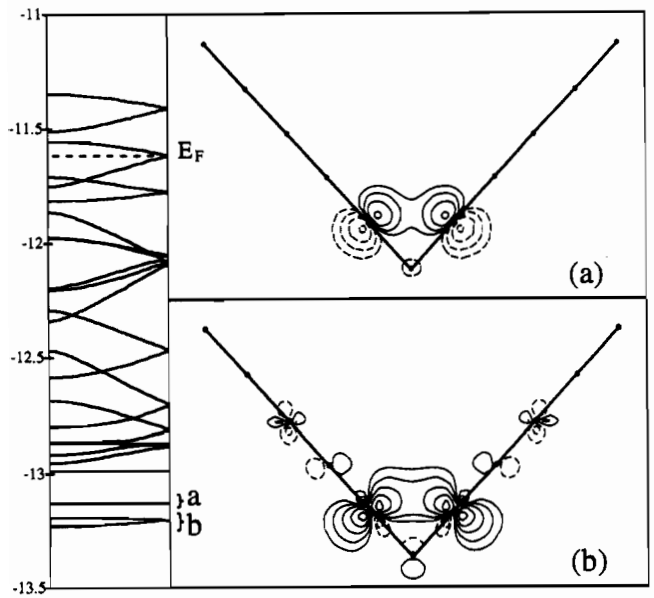

Figure 6. Band structure of BaNiN. Local orbitals (panels a and b) are labeled in correspondence with the bands from which they arise as indicated in the diagram at the left. Plot a is 0.26 Å above the plane of atoms, and plot b is in the atomic plane.

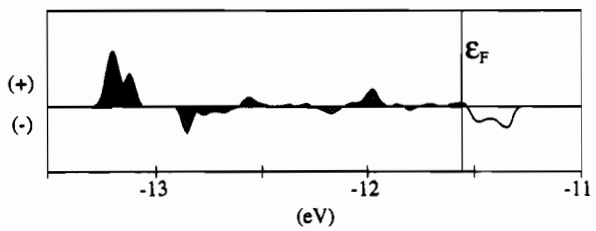

Figure 7. COOP curve for Ni–Ni interaction in BaNiN.

6a) is extremely well localized since the Ni d orbitals that constitute it have virtually no overlap with neighboring nitrogens, whether or not the chain is bent. The Wannier orbital with σ character (Figure 6b) is mainly Ni–Ni bonding with some small contributions from nearby atoms. The overlap population for a filling corresponding to a d^0 electron count is 0.029. Adding four electrons per Ni_3N_3 unit will fill the lower two folded bands shown in Figure 6 and gives an overlap population of 0.096, indicating a substantial σ interaction. Adding four more electrons will fill the next two bands, which were used in constructing Figure 6b, and yields an overlap population of 0.126.

The Wannier orbitals and overlap populations for these bands clearly imply the existence of a Ni–Ni bond. To investigate further, we examine the COOP curve shown in Figure 7. This COOP curve represents the differential overlap population between the two interacting nickel atoms. Notice the two bonding peaks just below –13 eV, which can be attributed to the bands from which we constructed the local orbitals in Figure 6. In order to understand what is happening above –13 eV, we need to look at the bending process further. As the chain is bent, the Ni d orbitals are split into two distinct symmetry sets, those symmetric with respect to the mirror plane retained by the chain ($x^2 - y^2$, z^2, xz) and those which are antisymmetric (xy, yz). When the bend is increased, significant orbital mixing will occur in regions where bands of the same symmetry overlap, or lie close in energy to each other. The bonding and antibonding peaks in the energy range –13 to –11.6 eV of the COOP curve represent interactions of mixed-orbital character, making a detailed analysis in this region tedious. We may avoid this difficulty by examining the Ni–Ni overlap population. The overlap population at the Fermi level (102 e^-) is 0.110. Since the overlap population for a filling just below –13 eV (56 e^-) is 0.126, the region between –13 eV and the Fermi level makes little net contribution to the Ni–Ni bonding. All of this indicates that there is a net bonding interaction between the Ni atoms and that the two lowest-lying bands are responsible for most of the bonding.

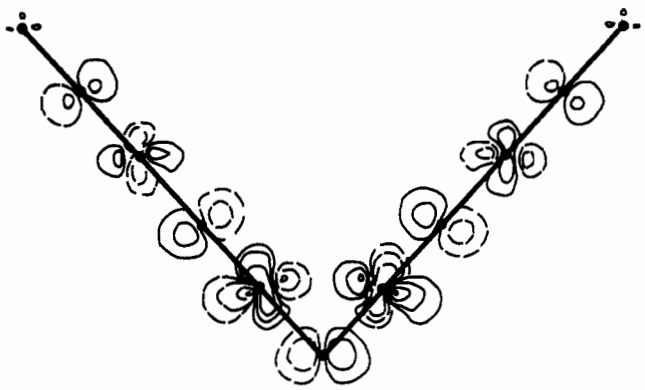

Figure 8. Local orbital showing σ^* character of the highest-lying band in Figure 6. This orbital is unoccupied.

More information is gleaned by the use of a hole formalism. The large antibonding peaks above the Fermi level represent antibonding bands which are not crossed by other bands of the same symmetry. It is therefore a simple matter to construct a local orbital for these bands (Figure 8). We may argue that since this band is unoccupied, there is a hole in the Ni–Ni σ^* orbital. We can thereby conclude that there is a net bonding interaction between the Ni atoms and that it is mainly σ in character.

Kniep and co-workers reported that the magnetic susceptibility of BaNiN was fit to a Curie–Weiss expression ($\chi_{molar} = (3N/k_B)\mu_{eff}^2/(T - \Theta)$) with Θ = 310 K and μ_{eff} = 1.0 μ_B. Of course, when susceptibility data are reported in terms of "μ_{eff}", an *interpretation* of the data has been appended—specifically, it has been assumed that one can speak of a magnetic moment per nickel center. However, if the susceptibility per Ni center is tripled, we have the susceptibility per Ni_3N_3 unit (which is the structural repeat unit). Then, since $\mu_{eff} \propto \sqrt{\chi}$, we conclude that μ_{eff} = 1.73 μ_B, which we can interpret as one localized spin per Ni_3N_3 unit. This admits two reasonable hypotheses about the "location" of the unpaired spin: it could be localized on the Ni centers that are bonded to two linear nitrogens, or it might be localized in the region of the Ni–N–Ni bends. There is no obvious site of electron localization, indeed the half-occupied band (indicated in Figure 6 as being bisected by the Fermi level) involves orbitals that have Ni–N π^* character and are quite delocalized over both types of Ni atoms. The magnetic properties of this material should receive more thorough experimental and theoretical investigation.

Nitridoferrates—Monomers, Dimers, and Chains

In our attemps to understand the iron nitride systems, we pay particular attention to possible Fe–Fe bonding along the Fe_2N_3 chains. Viewing $^1_\infty[(FeN_{3/2})_2^{5-}]$ chains as formed by the con-

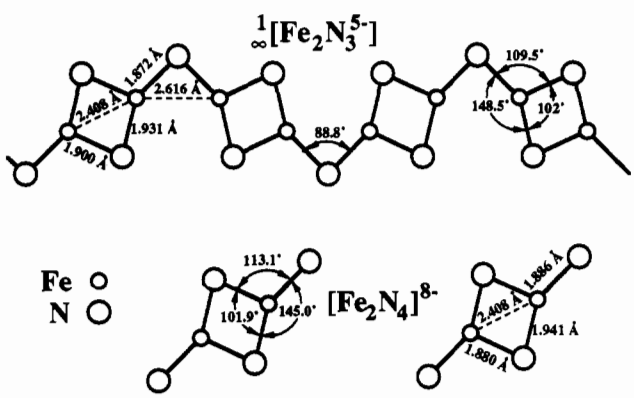

Figure 9. Structures of the $[Fe_2N_3]^{5-}$ chain and the $[Fe_2N_4]^{8-}$ dimer.

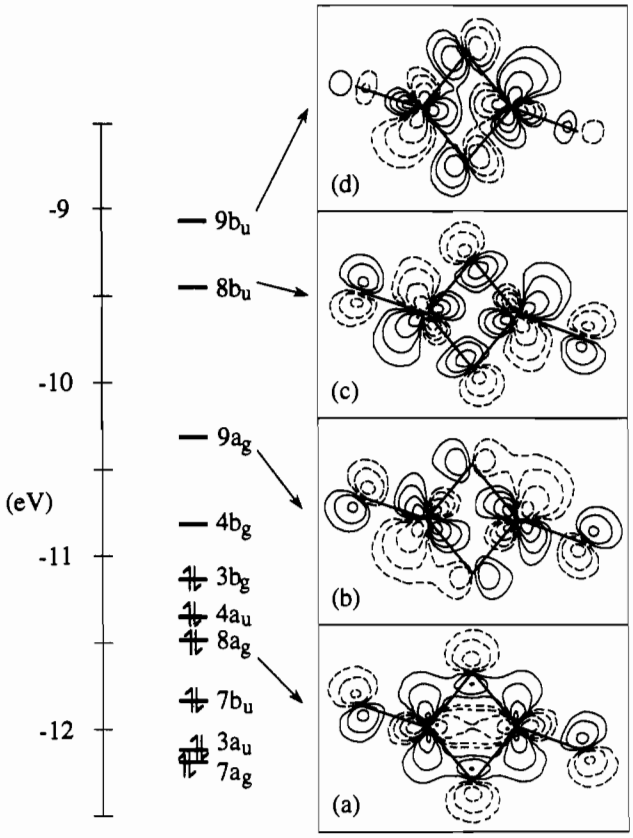

Figure 10. MO diagram and selected contour plots for $[Fe_2N_4]^{8-}$ d-based levels: (a) the $8a_g$ orbital of $[Fe_2N_4]^{8-}$ responsible for Fe–Fe bonding; (b) the $9a_g$ and (c) and $8b_u$ MO's (these MOs rehybridize to form Fe–Fe inter-ring bonds in the extended-chain compound); (d) the $9b_u$ orbital of $[Fe_2N_4]^{8-}$ which is Fe–Fe antibonding and unoccupied.

densation of $[Fe_2N_4]^{8-}$ units, we clearly expect the molecular identity of those units to be retained. This approach is bolstered by a careful structural examination of the two species as they are found in the compounds $Ca_2[FeN_2]$ and $Ba_2Li[Fe_2N_3]$ (Figure 9). Note that all bond lengths and angles are virtually identical in the $[Fe_2N_4]^{8-}$ ions and the corresponding subunits of the $^1_\infty[(FeN_{3/2})_2^{5-}]$ chains.

At the left in Figure 10 is a MO diagram showing the d-based levels of the $[Fe_2N_4]^{8-}$ ion. The lowest three MO's, $7a_g$, $3a_u$, and $7b_u$, are Fe–N nonbonding and have almost pure Fe d character. The other seven MO's are Fe–N antibonding in character. The lowest MO of these seven ($8a_g$) is principally responsible for Fe–Fe σ bonding within the dimer, while the highest MO ($9b_u$) has Fe–Fe σ^* character. There remains some question as to the electronic occupation of these levels. We believe that the $[Fe_2N_4]^{8-}$ ions possess no more than intermediate spin, since the levels $8b_u$ and $9b_u$ are separated by a sizable energy gap from the rest of the d manifold. No magnetic measurements have been carried

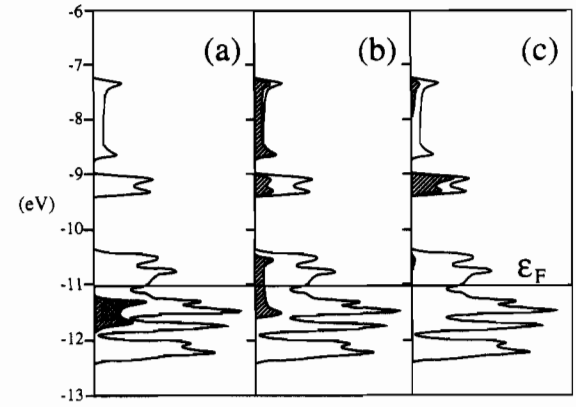

Figure 11. Total DOS along with shaded projections of certain molecular orbitals of the $[Fe_2N_4]^{8-}$ dimer as discussed in text: (a) projection for the $8a_g$ MO; (b) projection for the $9a_g$ and $8b_u$ MO's; (c) projection for the $9b_u$ MO.

out on compounds containing these ions, so experimental verification of our supposition is not available. We discuss the question of spin states further below.

Let us examine the MO's that are responsible for Fe–Fe bonding in the dimer and which are correctly oriented for Fe–Fe bonding between dimers. These are four key orbitals on which we focus in discussing the extended $^1_\infty[(FeN_{3/2})_2^{5-}]$ chain. These are the $8a_g$, $9a_g$, $8b_u$, and $9b_u$ MO's. Contours for these four molecular orbitals are plotted at the right in Figure 10. Looking at the plots in Figure 10a ($8a_g$) and Figure 10d ($9b_u$), we can see that these are the MO's which are σ and σ^* with respect to Fe–Fe bonding within the dimers. The orbitals plotted in Figure 10b ($9a_g$) and Figure 10c ($8b_u$) are the $[Fe_2N_4]^{8-}$ MO's which have the right spatial orientation for Fe–Fe bonding between Fe_2N_2 rings. These MO's have lobes on Fe atoms that point to where other Fe atoms are located in the ion's extended counterpart.

We now turn our attention to the $^1_\infty[(FeN_{3/2})_2^{5-}]$ chain. The calculated DOS for this system is plotted in Figure 11, along with some projected DOS curves to which we will refer below. Only the "d-band" region of the DOS is shown, and the Fermi level for a simple metallic ground state (all spins paired) is indicated. Perhaps the simplest place to begin our analysis is with the two highest-lying bands shown in Figure 11. These bands are not crossed by other bands, so it is easy to construct a Wannier orbital plot for each. The projected DOS plots in Figure 11 show the contribution to the chain DOS made by the four $[Fe_2N_4]^{8-}$ MO's plotted in Figure 10. These projections were obtained from a band structure calculation with a fragment molecular orbital analysis. The $^1_\infty[(FeN_{3/2})_2^{5-}]$ chain was partitioned into $[Fe_2N_4]^{8-}$ and $[Fe_2N_2]^{2-}$ units, and we have projected out the contributions of the MO's from the first fragment.

The Wannier orbital for the band centered at –9.2 eV is quite well localized on the Fe_2N_2 ring, with Fe–Fe σ^* character, and is clearly similar to the $9b_u$ MO for the $[Fe_2N_4]^{8-}$ ion (compare Figures 10d and 12a). Furthermore, the fragment orbital projections in Figure 11 show that this MO makes the largest contribution to this band. The broader, higher-lying band centered at –8.0 eV has significant Fe–Fe σ^* character with respect to metal–metal bonds *between* rings (Figure 12b) and derives from an admixture of the $9a_g$ and $8b_u$ MO's for the isolated $[Fe_2N_4]^{8-}$ ion (Figure 10b,c). From the projected DOS plots in Figure 11b, we infer that, on moving from the $[Fe_2N_4]^{8-}$ ion to the extended chain, these two molecular orbitals rehybridize and form the basis for the inter-ring Fe–Fe bonding and antibonding bands. This interpretation is easily demonstrated for the antibonding band by constructing the Wannier orbital shown in Figure 12b. (For the bonding counterpart to this orbital, we must overcome computational complications that arise when one tries to construct a single Wannier orbital from a band that crosses several other

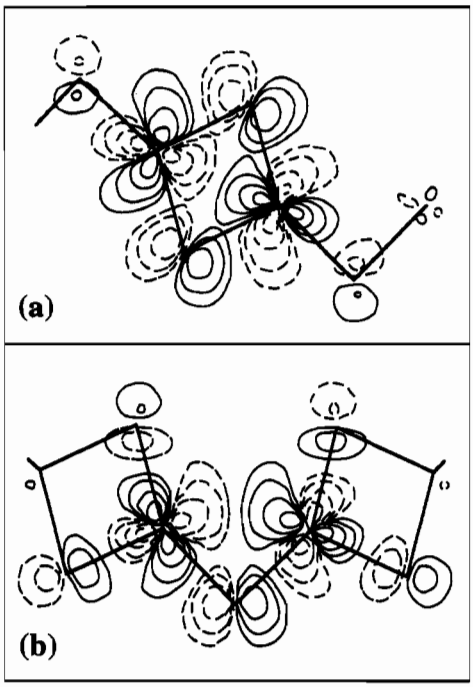

Figure 12. The (a) intra-ring and (b) inter-ring σ^* local orbitals derived from the two highest-lying bands in Figure 11. See text for discussion.

bands. We have a solution for these problems, but for the sake of brevity we will not further elaborate here.) Note that Figure 11b shows that the Fe–Fe inter-ring bonding band is bisected by the Fermi level ($\mathcal{E}_F = -11.03$ eV). The $8a_g$ MO for the $[Fe_2N_4]^{8-}$ ion (Figure 10a) is responsible for most of the Fe–Fe bonding in the isolated ion; the DOS projection of this orbital lies in a narrow energy range below the Fermi level and indicates that the intra-ring Fe–Fe bond is essentially unperturbed on moving from the discrete ion to the chain system.

Despite the fact that the extended Hückel method does not allow direct prediction of spin states, we can draw some conclusions by considering structural information in conjunction with our computed results. The short 2.40 Å Fe–Fe distances in both the $[Fe_2N_4]^{8-}$ ion and the intra-ring bonds of the $^1_\infty[(FeN_{3/2})_2^{5-}]$ chains are indicative of significant Fe–Fe bonding. It is therefore reasonable to assume that the intra-ring Fe–Fe σ^* orbital depicted in Figure 12a is completely *unoccupied*. Because this Wannier orbital was constructed from the band centered at –9.2 eV, the higher-lying band centered at –8.0 eV (inter-ring σ^* character, Figure 12b) must also be completely unoccupied, and we conclude that the longer 2.60 Å Fe–Fe distance between Fe_2N_2 rings also signifies important Fe–Fe bonding. (The calculated overlap populations for the two Fe–Fe contacts are comparable: 0.189 for the intra-ring Fe–Fe bond, 0.171 for the inter-ring Fe–Fe bond.) Clearly, if these bands are not occupied, high-spin Fe is ruled out for the chain compounds, and because of their close structural similarity, it is probably also ruled out for the $[Fe_2N_4]^{8-}$ ion. Even if a spin-polarized (magnetic) ground state holds for either of these systems, enough of the Fe-based electrons must remain paired to allow Fe–Fe bond formation. Some intermediate spin state, in which there is some net spin polarization in occupation of the bands between –12.4 and –10.4 eV, cannot be definitely ruled out. Still, we suspect that the extensive orbital delocalization of the "d orbitals" from iron to nitrogen will be associated with reduced effects of electron–electron repulsion and that a simple metallic state holds for the $M^{II}_2Li[Fe_2N_3]$ (M^{II} = Sr, Ba) compounds. We have discussed this line of reasoning more fully in our treatment of the FeN_3^{6-} ion.[11]

Concluding Remarks

We have noted that low transition metal coordination numbers are typical of the new nitridometalates. When interpreting these compounds' electronic structure within a ligand-field-theory framework, it is important to consider s–d hybridization from the ouset. Ligand-field orbital diagrams which fail to take s–d hybridization into account are likely to be *qualitatively* incorrect as to orbital energy orderings. This was evident in our earlier treatment of the MN_3^{6-} ions, in which a s–z^2 hybrid orbital lay low enough below M–N π^* orbitals that spin pairing in the former orbital occurred.[11] The focus of interest in the present work has not highlighted this point, but the reader may see the effects of s–d hybridization in each system we have studied by noting the existence of "extra" nonbonding orbitals. The highest occupied orbitals in all systems studied have M–N π^* character, and notwithstanding our introductory comments, the net M–N π bonding is not large for the nitridonickelates. The d-orbital manifold simply must accommodate too many electrons to leave many Ni–N π^* orbitals vacant.

The paucity of physical measurements for the new nitrides underlines the need for continued study of these structurally unusual compounds. Magnetic measurements would seem to be particularly needed to test our tentative conclusions about the transition metal spin states in these materials. We eagerly anticipate the unfolding of this chemistry.

Acknowledgment. We gratefully acknowledge the National Science Foundation for its support through a Presidential Young Investigator Award (Grant DMR-8858151) and the Robert A. Welch Foundation for its support through Grant A-1132.

Table I. Parameters for EH Calculations

	orbital	H_{ii}, eV	ζ_1[b]	ζ_2[b]	c_1[a]	c_2[a]
Fe	3d	–12.28	5.55	1.80	0.5366	0.6678
	4s	–9.22	1.90			
	4p	–5.37	1.90			
Ni	3d	–12.99	5.75	2.20	0.5817	0.5800
	4s	–8.86	1.92			
	4p	–4.90	1.92			
N	2s	–26.0	1.95			
	2p	–13.4	1.95			

[a] Coefficients used in double-ζ expansion. [b] Slater-type orbital exponents.

Appendix

The extended Hückel method was used for all band structure calculations; parameters appear in Table I. Structural parameters were idealized in the case of BaNiN, for which an average Ni–N bond length of 1.8 Å was used and angles slightly less than 180° were made linear. Band structure calculations were carried out by using a 50 k point mesh for a one dimension cell in all cases. All DOS curves were smoothed with Gaussian functions with a standard half-width of 0.03 eV.

In our analysis of bonding of extended systems, we have found it useful to construct local orbitals (Wannier functions) using a method analogous to that used to obtain bond orbitals in molecular systems.[23] To construct Wannier functions, we place a probe atom in an appropriate location, such as between the two interacting Ni atoms in BaNiN. We then calculate the overlap of this probe orbital with specific crystal orbitals. From this, it is possible to determine a phase factor by which we can multiply the crystal orbital, so as to build up electron density in the area of the probe orbital. The mathematical details are discussed in previous papers,[24–26] but we make the following points here. First, as for the relationship between bond orbitals and molecular orbitals, the local orbitals produce an electron density that is fully equivalent to that for the delocalized band orbitals from which the local orbitals are built. Second, when bonding is discussed for local orbitals, one should recall that identical orbitals are found in each unit cell of the crystal. For each band, there are as many delocalized band orbitals as there are unit cells of the crystals, but the former are delocalized over the entire crystal.

(23) Albright, T. A.; Burdett, J. K.; Whangbo, M.-H. *Orbital Interactions in Chemistry*; John Wiley & Sons: New York, 1985.
(24) Yee, K. A.; Hughbanks, T. *Inorg. Chem.* **1991**, *30*, 2321.
(25) Yee, K. A.; Hughbanks, T. *Inorg. Chem.* **1992**, *31*, 1620.
(26) Tian, Y.; Hughbanks, T. *Inorg. Chem.* **1993**, *32*, 400.